The vibrational excitations and the position of hydrogen in nanocrystalline palladium

1995 J. Phys.: Condens. Matter 7 219

(http://iopscience.iop.org/0953-8984/7/2/002)

J. Phys.: Condens. Matter 7 (1995) 219–230. Printed in the UK

The vibrational excitations and the position of hydrogen in nanocrystalline palladium

U Stuhr†‡, *H Wipf*†, *T J Udovic*§, *J Weißmüller*‖ *and H Gleiter*‖

† Institut für Festkörperphysik, Technische Hochschule Darmstadt, 64289 Darmstadt, Germany
‡ Hahn-Meitner Institut Berlin, BENSC-NI, 14109 Berlin, Germany
§ National Institute of Standards and Technology, Gaithersburg, MD 20899, USA
‖ Institut für Werkstoffwissenschaften, Universität des Saarlandes, 66123 Saarbrücken, Germany

Received 20 July 1994, in final form 14 September 1994

Abstract. *The vibrational excitations and the position of hydrogen in nanocrystalline palladium* were investigated by means of inelastic neutron-scattering and H solubility measurements. The study focuses on the H concentration regime ($\leqslant$ 4.8 at.% H) where, at room temperature, no precipitation of the H in a hydride phase (β-phase) was observed. In this concentration regime, the solubility measurements show an enhanced H solubility relative to coarse-grained Pd. The neutron-scattering experiments show that this additional H is incorporated in the grain boundaries and at the surface of the grains. Surface modes of H at $\sim$ 90 and 120 meV were identified. Compared to coarse-grained Pd, no change in the H solubility was found for the crystal lattice of the nanosized grains.

1. Introduction

The analysis of the vibrational frequencies of hydrogen, as determined by inelastic neutron scattering, is an established method to investigate H sites in metals [1–3]. Furthermore, this method has been used to study H precipitation [4], the lattice potential of the H [5–7] and its local environment in disordered materials such as metal glasses [8]. Although most of these experiments investigated bulk properties, some investigations of H at metal surfaces have been reported as well [3, 9, 10]. In the present study we investigated the neutron spectra of H vibrations in nanocrystalline palladium (n-Pd).

Nanocrystalline materials are polycrystals with a grain size in the range of a few ($\sim$ 2–30) nanometres. In such a material the number of atoms within the grains, which have a periodic crystalline surrounding, is comparable with the number of atoms in grain boundaries or at internal surfaces. The second group of atoms has an (at least partly) disordered local surrounding [11–13]. In the last two decades several methods have been developed to produce nanocrystalline material with high purity. One of the most important methods is the inert gas condensation process [11, 12, 14].

In contrast to H in conventional (coarse-grained or single-crystalline) Pd, which is one of the most extensively investigated metal–H systems, only little is known about H in n-Pd. Some properties of H in n-Pd were reported in studies on the solubility [15–17] and the chemical diffusion of the H [15]. From these studies it is known that, for low H concentrations, the H solubility of n-Pd is higher than that of coarse-grained Pd. However, it was not conclusively established which sites these additional H atoms occupy. Whereas the authors of [15] and [16] suggest that the additional H occupies sites at grain boundaries,

0953-8984/95/020219+12$19.50

the authors of [17] argue in favour of a size-dependent increased solubility in the crystal lattice, which implies a homogeneous distribution of the additional H on lattice sites.

In this paper we report results (i) of H-solubility measurements of n-Pd and (ii) a neutron-spectroscopy study, which investigates the vibrational modes of the H. Our interest in this study focuses on low H concentrations ($\leqslant$ 4.8 at.%) where, for the H in the grains, no precipitation of the β-phase occurs at room temperature. The motivation of the study was to identify the sites of the incorporated H and to investigate their potential.

2. Experimental details

We investigated pure and H-doped n-Pd and, for comparison, coarse-grained Pd samples. The n-Pd was produced from Pd wire (nominal purity 99.95%), using the inert gas condensation method [11, 12, 14]. The samples were prepared in a high-vacuum (HV) apparatus in a pure helium gas atmosphere. The Pd was evaporated from a tungsten boat by resistivity heating. The nanocrystalline powder produced in the He atmosphere precipitated on a liquid-nitrogen-cooled cold finger. From this finger it was scraped and gathered in a small pot. After the production of about 0.2 g of n-Pd powder, the chamber was evacuated (below 2×10^{-7} mbar; 1 mbar = 100 Pa) and the powder was compressed hydraulically at a pressure of about 0.7 GPa. The resulting discs had diameters of 8 mm. The samples were stored in an argon atmosphere to prevent contamination with oxygen.

The grain size was determined from the width of the (111) Pd reflection measured with x-rays [18]. For the neutron-scattering experiments only samples with an average grain size of less than 23 nm were used. The total amount of n-Pd used in the neutron-scattering experiment was 3.1 g; the average grain size was about 15 nm.

One of the discs, which was not used for neutron scattering due to its larger grain size, was used to investigate the H solubility of n-Pd. The x-ray measurement of this sample yielded a grain size of 38 nm; the mass of this disc was 0.23 g. The solubility was measured at room temperature (293 K) in a UHV apparatus with calibrated volumes and differential membrane manometers. The supplied H was purified in a Pd permeation cell.

For the neutron-scattering runs and the H charging, the sample was kept in an aluminium container which—for H doping—could be connected to an external HV apparatus. This prevented sample contact with air. The sample was in contact with air only during the x-ray measurement. Nevertheless a mass spectrometer showed that a small amount of H_2O gas was produced during the first H loading of the sample, an effect also reported previously for coarse-grained Pd [19]. During several charging and degassing cycles of the sample with small amounts of H, the produced H_2O was gathered in a cold trap until no more H_2O was detected. Then, the apparatus was evacuated. The total amount of caught H_2O, which was equivalent to 0.7 at.% H, was calculated from the pressure in the apparatus after warming up the cold trap. The H loading of the sample was carried out at room temperature and the concentration was determined by standard volumetric methods.

The neutron spectra of the n-Pd sample were taken before and after doping with 2.4 and 4.8 at.% H. At the first loading, the equilibrium pressure was 1.4 mbar; the second one was stopped at an H pressure of 12.9 mbar. After the first loading, an H concentration of 2.4($\pm$0.4) at.% was determined; after the second loading the hydrogen concentration was 4.8($\pm$0.5) at.%.

For comparison, a second sample of coarse-grained Pd was prepared. The sample was kept in an identical sample container as the n-Pd. The mass of the Pd was 12.6 g and the H concentration was 0.6 at.%. Therefore the total amount of H in this sample was about the

same as that in the n-Pd sample at 2.4 at.%. Due to the low H concentration of 0.6 at.%, the sample was in the pure α-phase region at room temperature [20,21].

The neutron spectra were measured with the BT4 spectrometer at the National Institute of Standards and Technology (NIST), using the Cu(220) monochromator with 60′–40′ collimation and a beryllium filter for the energy analysis of the scattered neutrons. The energy resolution of this instrument increases from about 4 meV (full width at half maximum, FWHM) for neutron energy losses below 40 meV to about 10 meV at the highest investigated energy transfers of about 140 meV. During the neutron-scattering experiments, the samples were kept in a closed-cycle refrigerator with a temperature stability of about 1 K.

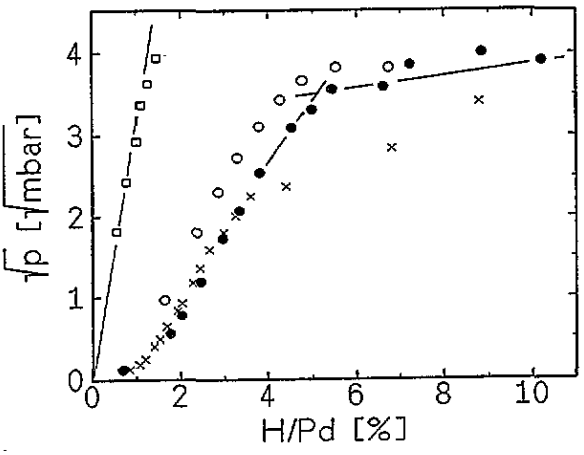

Figure 1. H solubility curves of a nanocrystalline sample with an average grain size of about 38 nm and of a coarse-grained sample. The square root of the equilibrium pressure at 293 K is plotted against the H/Pd atom ratio. The closed circles represent the first doping of the sample, the crosses the desorption after the first doping, and the open circles the second doping procedure of the sample. The values of the coarse-grained sample are given by the open squares. For more details, see the text.

3. H solubility of nanocyrstalline Pd

Figure 1 shows a plot of the square root of the H equilibrium pressure versus the H/Pd atom ratio. The closed circles represent the values for the first doping of the sample, the crosses those for the subsequent H desorption, and the open circles those for a second doping process. The open squares were measured after converting the nanocrystalline structure of a sample into a coarse-grained morphology by heating it to $\sim$ 1200 K. These data points follow Sieverts' law, which predicts the H solubility to be proportional to the square root of pressure, and are in good agreement with previous H-solubility experiments on coarse-grained Pd [20–22].

Figure 1 shows that the H solubility of the nanocrystalline sample is much higher than that of the coarse-grained Pd. Further, Sieverts' law is not followed by the n-Pd sample, even at the lowest H concentrations. Both results are qualitatively in agreement with previous room-temperature results [15, 17]. Above an H concentration of about 5.2 at.%, the equilibrium pressure (at about 12 mbar) does not significantly vary with increasing concentration. The time required to reach approximately equilibrium conditions increased from several minutes at low concentrations to nearly a day for concentrations above 5.2 at.%. Both facts, the approximately constant equilibrium pressure and the slow H absorption, indicate that the miscibility gap between the solid solution α-phase and the β-phase is reached at 5.2 at.%. This concentration is about five to ten times higher than the values

reported for coarse-grained Pd [20]; however, the equilibrium pressure [20–22] remains nearly unchanged. It should be noted that Mütschele and Kirchheim [15] report a value twice as large for the concentration marking the onset of the miscibility gap, although for a sample with a much smaller grain size (5 nm).

After the first doping and desorption, the sample was evacuated at 1.4×10^{-8} mbar for about 17 h and subsequently a second solubility measurement was carried out. The results of this measurement are represented by the open circles. The solubility curve resulting from this second doping procedure has the same shape as that of the first doping, but is slightly shifted to smaller concentrations by approximately 0.7 at.%, whereas the doping and desorption curves of the first doping cycle do not significantly differ from each other. This indicates that not all of the H could be removed. About 0.7 at.% H was probably trapped in the sample and could not be extracted at room temperature.

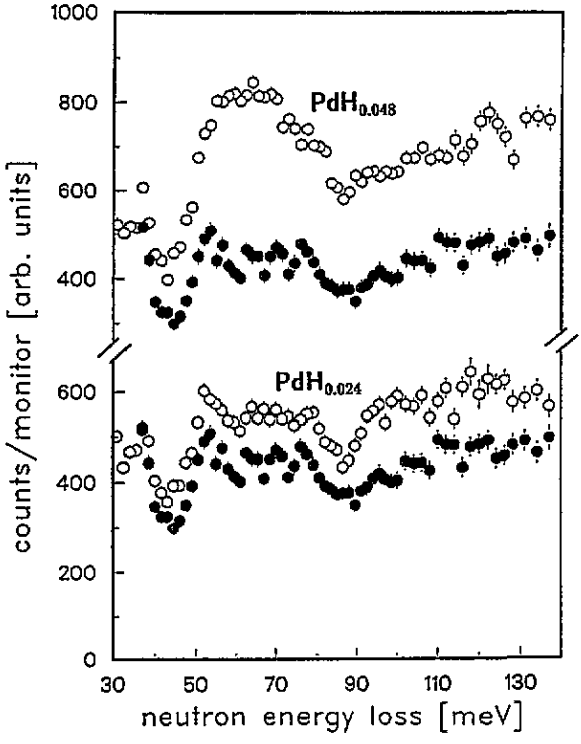

Figure 2. Neutron energy-loss spectra of the n-PdH_x samples at 10 K. The spectra of the H-doped samples are shown by the open circles and those of the undoped sample by the closed ones. In the upper part of the figure the spectrum with the higher H concentration ($x = 0.048$) is shown, in the lower part the spectrum with the lower concentration ($x = 0.024$). The ordinate shows the neutron counts divided by the monitor counts in arbitrary units.

4. Neutron-scattering results and discussion

4.1. Neutron spectra

Figure 2 shows neutron spectra of the H-doped nanocrystalline sample taken at 10 K for the two H concentrations of 4.8 at.% and 2.4 at.% in comparison to the spectra of the undoped n-Pd sample. These spectra were all taken with the same sample and sample container, only the H concentration varied. This assures that the background is the same for all spectra.

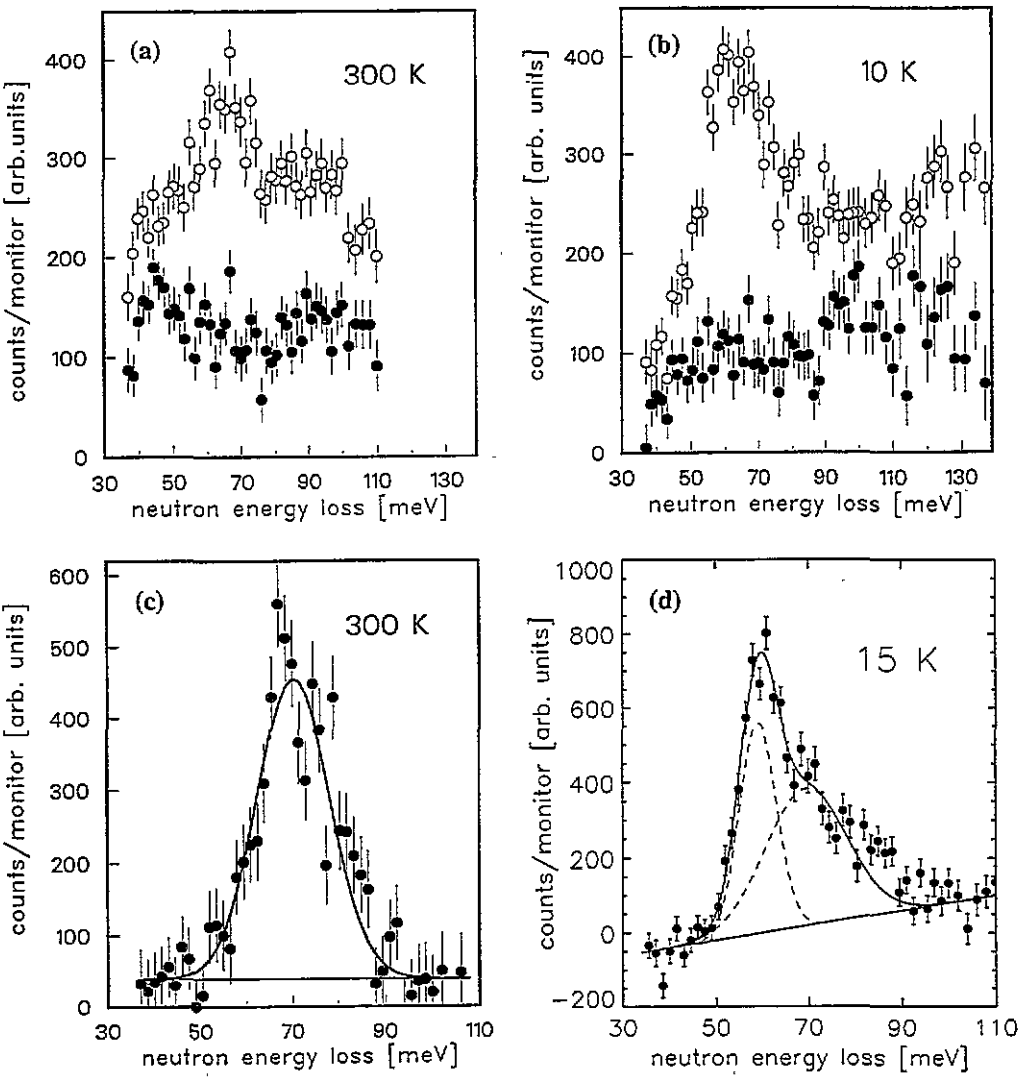

Figure 3. Spectra of the H modes. The spectra of the undoped samples are subtracted from those of the H-doped samples. The spectra of the n-Pd sample are shown at (a) 300 K and (b) 10 K. The closed circles represent the spectra of the sample with low H concentration (2.4 at.%), the open circles the spectra of the high H concentration (4.8 at.%). The spectra of the coarse-grained sample are shown at (c) 300 K and (d) 15 K. The full lines are fits with one (300 K spectrum) and two (15 K spectrum) Gaussian functions. The broken lines are the individual Gaussian functions plus background.

In order to improve the visibility of the H modes, the spectra of the undoped samples were subtracted from the spectra of the doped samples. The resulting spectra are shown in figure 3. However, along with the background the modes of any possible small amount of residual H are also eliminated in these spectra. Therefore, all further conclusions apply only for the added H, not for any residual H. Figures 3(a) and (b) show the 300 K and the 10 K spectra, respectively. In these figures the open circles show the spectra for the higher H concentration of 4.8 at.% and the closed circles those for the lower concentration

of 2.4 at.%. For comparison, the spectra of the coarse-grained $PdH_{0.006}$ sample at 300 K and at 15 K are presented in figures 3(c) and (d), respectively. The spectra of the doped and undoped coarse-grained sample at 15 K were taken one year later, so that the intensity and the background are not comparable to the other spectra.

In figure 3(c) the spectrum of the undoped nanocrystalline sample was taken as background and was subtracted from the spectrum of the polycrystalline sample. Although the spectra were taken from different samples, the background subtraction matches perfectly, which shows that the background has mainly an instrumental origin and is not caused by any impurities of the n-Pd sample.

The most striking contrast between the spectra of the H-doped n-Pd samples is that the spectra for $x = 0.048$ exhibit an intense peak in the energy range of 50–80 meV whereas the spectra for $x = 0.024$ have only little structure. The peaks of the spectra for $x = 0.048$ coincide with the peaks of the coarse-grained sample as well as with the optical modes of H in Pd reported in previous studies [4, 23–26]. Consequently, these modes are attributed to the H in the crystalline regions of the grains. In the spectra of the n-PdH_x sample with $x = 0.024$, no discernible peaks have been noticed in this energy region. Apparently, for this H concentration only a minor part of the H is located in the crystalline regions of the grains. Hence, up to this concentration the H prefers sites in the grain boundaries and/or at inner surfaces of the sample.

The total amount of H in the n-$PdH_{0.024}$ sample was approximately the same as that in the coarse-grained $PdH_{0.006}$. In coarse-grained Pd this H has only one vibrational frequency, represented by the mode shown in figure 3(c). Therefore, if all hydrogen modes of the n-PdH_x are in the investigated energy range a value of about one can be expected for the ratios of the integrated intensities of the H modes of the n-$PdH_{0.024}$ and of the coarse-grained sample. At the higher concentration (n-$PdH_{0.048}$) a value of about two may be expected.

Table 1. Integrated intensities of the spectra shown in figure 3, divided by the intensity of the coarse-grained (CG) sample. The field, 'range of integration', shows the energy range over which the spectra are integrated. The amount of H in the n-$PdH_{0.024}$ is about the same as that in the coarse-grained Pd sample $PdH_{0.006}$. The quoted errors represent only the statistical uncertainties.

Spectrum	Range of integration (meV)	Relative intensity
CG $PdH_{0.006}$ (300 K)	37–108	1.0
n-$PdH_{0.024}$ (10 K)	37–110	0.68 ± 0.04
	37–140	0.98 ± 0.06
n-$PdH_{0.024}$ (300 K)	37–110	0.85 ± 0.05
n-$PdH_{0.048}$ (10 K)	37–110	1.67 ± 0.08
	37–140	2.35 ± 0.12
n-$PdH_{0.048}$ (300 K)	37–110	1.80 ± 0.09

Table 1 lists the integrated intensities of the spectra in figure 3 divided by the intensity of the coarse-grained $PdH_{0.006}$ spectrum at 300 K. Two different integration ranges are used as indicated in the table. The quoted errors reflect the calculated statistical errors. However, in order to gain some physical insight we have to compare neutron intensities for the same amount of H. For this purpose we have also to consider other uncertainties such as those in the H concentrations of the n-Pd sample. A further uncertainty results from the fact that for the 300 K spectra of the n-Pd sample, the spectra of the undoped sample taken at 10 K are subtracted. Despite these uncertainties, the data in the table confirm that the total integrated intensities found are in the expected range for all spectra. This demonstrates that the energies of at least the major part of the optical H vibrations of the n-PdH_x are in the

investigated energy range. However, note that this does only apply to the 10 K spectra if we expand the integration range up to 140 meV.

The spectra of the n-$PdH_{0.024}$ sample at 10 K in figures 2 and 3(b) show that most of the H-induced intensity occurs in the energy region between 90 meV and 140 meV, with a maximum at about 95 meV and possibly a second one at 125 meV. The 300 K spectra show the same effect, but less pronounced. Only one broad peak at about 90 meV can be observed. However the peak at 90 meV has less intensity then the two peaks in the spectrum at 10 K.

Let us now first discuss the origin of the modes between 90 meV and 140 meV. In the following subsections the modes of the H in the crystalline regions of the grains will be addressed and this section will close with some general discussions of our results.

4.2. The H modes above 80 meV

In order to identify the H modes of n-PdH_x found above those of the coarse-grained PdH_x, we compare our neutron spectra with results for H modes in other nanostructured Pd (Pd black [9, 10, 27], Raney Pd [28], and adsorbed Pd in zeolites [29]) and of adsorbed H on Pd surfaces [30–32]. For H on Pd black two peaks at 94 and 120 meV were found by neutron spectroscopy. These peaks were attributed to dissociated surface H atoms vibrating parallel and perpendicular to the surface [9, 10]. The same modes were found in high-resolution electron energy-loss spectroscopy (HREELS) studies of H adsorbed on a (111) surface (96 meV and 124 meV, [30]) and a (110) surface (98 meV and 120 meV, [32]) of Pd single crystals. For H on a (100) surface, however, only modes in the energy range of 50–80 meV were found [31]. Modes with energies of 92 and 132 meV for H on Raney Pd [28] and modes at 80–110 meV and 128 meV for H on Pd in zeolites [30] were found by neutron spectroscopy. In these studies, however, the H modes between 80 and 110 meV were attributed to H on so-called subsurface sites, i.e. sites between the first and second atom layers of a surface. The assignment of these modes to H on subsurface sites is also supported by recent theoretical work [33], in which the H modes on a (111) surface of Pd were calculated, yielding vibrational energies of 99 meV for H in subsurface sites and 118 meV for H on surface sites.

These previous experimental and theoretical studies show that the H modes in the range of 90–100 meV and near 120 meV can be attributed to H on or near the Pd surface. The spectra of the n-$PdH_{0.024}$ sample show maxima at nearly exactly these energies, at 100 meV and 120 meV. Therefore, these modes can be attributed to modes of H on sites at inner surfaces of the material or from H on those sites in the grain boundaries with a potential shape similar to those of the surface sites. According to this interpretation, it is not surprising that the modes are broadened compared to those measured on Pd black, because, in grain boundaries, the environment of the H atoms, and hence their potential, is expected to vary much more than on a surface. The broad backgrounds in the spectra in figures 3(a) and (b) are proposed to originate from H vibrational modes at grain boundary sites with different shapes of the interatomic potential.

The spectrum of the sample with $x = 0.048$ at 10 K in figure 3(b) shows an increase in the intensity at 120 meV. However, probably most of these additional excitations are not surface modes, but modes of two-phonon processes of the optical modes at 60 meV. An intensity estimation for two-phonon processes supports this conclusion.

4.3. Modes of the H in the crystalline regions of the sample

Figure 4 shows difference spectra of the n-PdH_x sample for the two investigated H concentrations, measured at 300 K and 10 K The spectra taken at the lower concentration

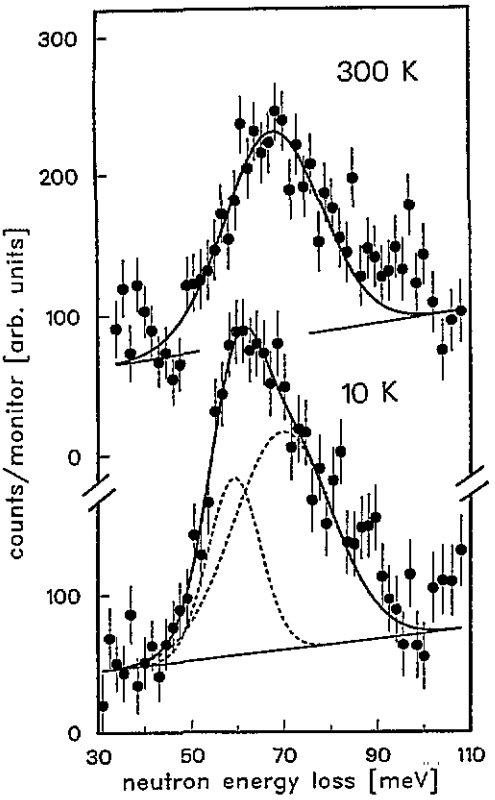

Figure 4. Difference spectra of the n-PdH_x spectra with $x = 0.048$ and $x = 0.024$. The full lines are fits with one (300 K spectrum) and two (10 K spectrum) Gaussian functions. The broken lines are the individual Gaussian functions plus background. For details, see the text.

($x = 0.024$) were subtracted from the spectra obtained at the higher H concentration ($x = 0.048$). For an analysis of the peaks of the n-PdH_x sample with $x = 0.048$, there are two advantages using these difference spectra rather than the spectra shown in figures 2 and 3. Firstly, the spectra with $x = 0.024$ were taken with better statistics than the spectrum without H. Secondly, the difference spectra of figure 4 are composed of spectra taken at the same temperature, which was not possible for the spectrum in figure 3(a), since no 300 K spectrum was available for the undoped sample.

For a quantitative analysis, the spectra in figures 4 and 3(c) and (d) were fitted by means of Gaussian functions. All spectra display a small shoulder on the high-energy side of the peaks, which can be attributed to two-phonon processes [4]. To avoid any contributions from these two-phonon processes, the energy range of the fits was restricted to data points below 82 meV. For the fits, a fixed linear background for each spectrum, as shown in the figures, was used. Since it was not possible to fit the peaks in the spectra at 10 K with a single Gaussian function, two Gaussian functions were used. The fits and the chosen background are shown in the figures by the solid lines and the broken lines in figures 4 and 3(d) show the contribution of the individual Gaussians to the fits.

The fit results are compiled in table 2. The intensities listed are the integrated intensities without background, divided by the intensity (again without background) of the corresponding difference spectrum of the coarse-grained sample at 300 K (figure 3(c)).

For the H mode in coarse-grained Pd at 300 K, the results for the energy (70.3±0.8) meV and the linewidth (~ 19 meV) are in good agreement with the results of previous experiments on H modes in the α-phase of Pd [4, 25]. At 10 K, the H is in the β-phase. Compared

Table 2. Fit results of Gaussian functions to the difference spectra n-$PdH_{0.048}$ − n-$PdH_{0.024}$ and the difference spectra for the coarse-grained sample $PdH_{0.006}$ − Pd and $PdH_{0.006}$ − n-Pd at 300 K and 10 K, respectively. The intensities of the n-PdH_x spectra are divided by the intensity of the best fit of the $PdH_{0.006}$ spectrum at 300 K. For details, see the text.

Spectrum	Centre of the peak (meV)	Linewidth (FWHM, meV)	Relative intensity
CG $PdH_{0.006}$ (300 K)	70.3 ± 0.8	18.6 ± 1.9	1.0
CG $PdH_{0.006}$ (10 K)			
peak 1	59.1 ± 0.4	9.5 ± 1.0	$(41 \pm 11)\%$
peak 2	69.4 ± 2.0	20.7 ± 3.5	$(59 \pm 11)\%$
n-$PdH_{0.048}$ (300 K)	67.7 ± 1.2	25.5 ± 4.0	0.51 ± 0.13
n-$PdH_{0.048}$ (10 K)			0.73 ± 0.18
peak 1	59.2 ± 1.7	13.0 ± 3.5	0.22 ± 0.11
peak 2	69.6 ± 3.5	25.1 ± 4.2	0.51 ± 0.18

with the spectrum at 300 K, the H mode is shifted to lower energies and a distinct shoulder on the high-energy side of the peak appears. This shoulder can be attributed to a strong dispersion of the optical mode in the β-phase [24, 26]. The values for the maximum and the shape of the peak again are in good agreement with previously published results [4, 24].

The peak in the 10 K spectrum (figure 4) is shifted to lower energies compared to the spectrum at 300 K. At 300 K, the peak for the difference spectrum of the n-PdH_x sample (spectrum of the low concentration $x = 0.024$ subtracted from the spectrum for $x = 0.048$) has its centre at about 67 meV and a linewidth of about 25 meV. The position of the peak agrees well with the results for H in the α-phase of coarse-grained PdH_x in former studies [4, 25] and of the coarse-grained sample used in this study. Thus, this peak is attributed to the H in the crystalline regions of the grains.

From a comparison of the spectral intensities the amount of H located in the grains of the n-Pd sample can be determined. At 300 K, the increase of the total H concentration from 2.4 at.% to 4.8 at.% caused an increase of (1.2 ± 0.3) at.% H in the grains. This means that about half of the additional H atoms occupy sites in the grains and half occupy other sites.

With these results, we can compare the solubility of the grains in n-Pd with those of coarse-grained Pd. At 300 K and a pressure of 12.9 mbar, the conditions at which the n-Pd sample was loaded to 4.8 at.%, the H solubility of coarse-grained Pd is about 1.0 at.% [20, 21]. This agrees well with the lattice H concentration of the n-$PdH_{0.048}$ sample derived from the neutron spectra. Hence, it is concluded that the reduction of the crystal size to the nanometre scale has little effect on the solubility of the H in the Pd lattice. This conclusion is supported by the absence of a peak in the 50–80 meV region of the 300 K spectrum for n-$PdH_{0.024}$. This sample was doped at a pressure of 1.4 mbar, corresponding to a lattice H concentration of 0.3 at.%, if the lattice solubility is identical to that in coarse-grained Pd. In this case, only one-eighth of the total amount of H dissolved in the nanocrystalline sample is located on lattice sites, and no discernible peak is expected from this small quantity. In agreement with this reasoning, no 70 meV peak is observed in this sample. Hence, both the absence of the 'lattice H peak' and the presence of excitations characteristic of H on interface sites support the conclusion that the major part of the H is located in the grain boundaries of n-$PdH_{0.024}$. This implies that the increased H solubility of n-Pd compared to coarse-grained Pd, as demonstrated in figure 1, is caused by the high solubility of the grain boundaries.

The peak in the n-Pd spectrum at 10 K in figure 4 again is shifted to lower energies. Figure 4 and the fit results show that the position of the first peak is identical to that in the

spectrum of the coarse-grained sample at 10 K, and is therefore attributed to the H in the β-phase in the grains. However, the shapes of the two spectra are significantly different. The shoulder is somewhat higher in the nanocrystalline sample, which is also represented by the fit results in table 2.

The intensity of this H mode in the 10 K spectrum is a little higher than that in the 300 K spectrum. However, most of this increase of intensity can be explained by (i) an increase of intensity caused by the lower frequency of the local vibration and (ii) a decrease of the Debye–Waller exponent due to the lower sample temperature. Therefore, cooling of the sample caused no significant change of the H concentration in the grains.

In both spectra in figure 4, the peaks of the n-$PdH_{0.048}$ sample are slightly broadened compared to the modes in coarse-grained Pd in figures 3(c) and (d). The reason for this might be an effect of the internal strains in the grains, such as also reported in a previous x-ray study [34]. These internal strains modulate the H potentials and therefore the H modes; hence, the averaging over many potentials causes a line broadening. However, although the peaks are slightly broadened, their position is not significantly shifted. Therefore, an increase of the local vibration modes caused by surface tension as reported in [35] cannot be detected.

4.4. General discussion

Let us examine the implications of the results of the present study for the controversial discussion, in [15], [16], and [17], on the origin of increased H solubility in n-Pd. From measurements of solubility as a function of chemical potential, Muetschele and Kirchheim attribute the excess H solubility before the onset of β-phase precipitation in n-Pd compared to coarse-grained Pd to H in a disordered Pd grain-boundary phase. From the unchanged chemical potential at the onset of β-phase formation, the authors conclude upon identical lattice solubilities in coarse-grained and nanocrystalline Pd. In a second study, Eastman *et al* [17] interpret x-ray lattice constants in terms of an increase in solubility, comparable in magnitude to the one reported in [15] and [16]. In contradiction with that work, the increased solubility is attributed to a (grain-size-dependent) change of the thermodynamic functions of the lattice, that is, the excess H is argued to be located in a homogeneous solid solution in the lattice, as opposed to grain-boundary segregation sites.

The results of the present study constitute unambiguous evidence of the presence of at least two different types of hydrogen site, interstitial sites in the lattice and grain-boundary ones. These sites differ with respect to their vibrational properties and with respect to their potential energy: some grain-boundary sites are occupied at lower chemical potential than lattice sites. Our results indicate that H in the grain-boundary sites can account for the entire increase of overall solubility. These results agree with the interpretation proposed by Mütschele and Kirchheim [15], i.e. increased solubility of H in the grain boundaries. They are also in accordance with the increase of solubility in nanocrystalline alloys recently been predicted on the basis of theoretical models of their overall thermodynamic functions [36,37]. On the other hand, our result appears not to be compatible with the interpretation by Eastman *et al* [17].

We shall speculate shortly upon possible explanations for this disagreement. Although we observe no increase in H concentration in the lattice sites, the lattice constant in the particle centres may be shifted by long-range strain fields, originating from regions near the grain boundaries where the H concentration deviates markedly from that in the interior of the crystallites. Alternatively, the presence of such regions may merely shift the measured lattice constant, which is an average over the regions close to the grain boundaries and the interior of the crystals. Note also that the H sites we labelled 'grain-boundary sites' because

of their characteristic vibrational and energetic properties may at the same time be lattice sites of the H sublattice from a crystallographic point of view, i.e. surface or subsurface sites. These sites have lattice positions, but have electronic and vibrational properties different from the ones in the bulk. Even if H occupies non-lattice sites, this does not necessarily imply disorder in the host (Pd) lattice, in analogy to the case of free surfaces, where the atomic short-range order of adsorbate layers is often fundamentally different from that of the substrate. Hence, as x-ray scattering in Pd–H arises practically exclusively from Pd, the segregated H may escape detection by x-ray-scattering techniques. The considerations in this paragraph imply that, although our results disagree with some conclusions in [17], they appear to be compatible with the x-ray-scattering data in that work.

5. Conclusion

We investigated the H solubility and the vibrational modes of H in nanocrystalline Pd. The analysis of the data allowed the determination of the location of the H. Up to an H concentration of about 2 or 3 at.% the H is found to occupy primarily sites in grain boundaries and at inner surfaces of the material. H modes attributed to H on sites similar to those at Pd surfaces are found. If the H concentration is increased above 3 at.% the H occupies also sites in the crystalline regions of the grains. The H solubility in these crystalline regions seems unchanged relative to coarse-grained Pd.

The selective incorporation of H in grain-boundary sites can be utilized in future experiments. The H, aided by its its high incoherent neutron-scattering cross-section, can be used as a probe to investigate the dynamics in the grain boundaries of nanostructured materials by neutron spectroscopy.

Acknowledgments

This work was financially supported by the Bundesministerium für Forschung und Technologie and the Deutsche Forschungsgemeinschaft (DFG).

References

[1] Springer T 1978 *Hydrogen in Metals I (Topics in Applied Physics 28)* ed G Alefeld and J Völkl (Berlin: Springer) p 75
[2] Springer T and Richter D 1987 *Methods of Experimental Physics* vol 23, part B, ed D L Price and K Sköld (London: Academic) p 131
[3] Richter D, Hempelmann R and Bowman R C Jr 1988 *Hydrogen in Intermetallic Compounds II (Topics in Applied Physics 67)* ed L Schlapbach (Berlin: Springer) p 97
[4] Magerl A, Rush J J, Rowe J M, Richter D and Wipf H 1983 *Phys. Rev.* B **27** 927
[5] Rush J J, Rowe J M and Richter D 1984 *Z. Phys.* B **55** 283
[6] Eckert J, Goldstone J A, Tonks D and Richter D 1983 *Phys. Rev.* B **27** 1980
[7] Hempelmann R, Richter D and Price D L 1987 *Phys. Rev.* B **58** 1016
[8] Rush J J, Rowe J M and Maeland A J 1980 *J. Phys. F: Met. Phys.* **10** L283
[9] Nicol J M, Rush J J and Kelly R D 1987 *Phys. Rev.* B **36** 9315
[10] Nicol J M, Rush J J and Kelly R D 1988 *Surf. Sci.* **197** 67
[11] Gleiter H 1989 *Prog. Mater. Sci.* **33** 223
[12] Siegel R 1991 *Material Science and Technology* vol 15, ed R W Cahn, P Haasen and E J Kramer (Weinheim: VCH Verlagsgesellschaft) p 583
[13] Gleiter H 1992 *Adv. Mater.* **4** 474

[14] Granqvist C G and Buhrman R A 1976 *J. Appl. Phys.* **47** 2200
[15] Mütschele T and Kirchheim R 1987 *Scr. Metall.* **21** 135
[16] Mütschele T and Kirchheim R 1987 *Scr. Metall.* **21** 1101
[17] Eastman J A, Thompson L J and Kestel B J 1993 *Phys. Rev.* B **48** 84
[18] Krivoglaz M A 1969 *Theory of X-Ray and Thermal-Neutron Scattering by Real Crystals* (New York: Plenum)
[19] Lynch J F and Flanagan T B 1973 *J. Phys. Chem.* **77** 2623
[20] Wicke E and Nernst G H 1964 *Ber. Bunsenges. Phys. Chem.* **68** 224
[21] Clewley J D, Curran T, Flanagan T B and Oates W A1973 *J. Chem. Soc. Faraday Trans.* I **69** 449
[22] Brodowsky H and Poeschel E 1965 *Z. Phys. Chem., NF* **44** 143
[23] Chowdhury M R and Ross D K 1973 *Solid State Commun.* **13** 229
[24] Hunt D G and Ross D K 1976 *J. Less-Common Met.* **49** 169
[25] Drexel W, Murani A, Tocchetti D, Kley W, Sosnowska I and Ross D K 1976 *J. Phys. Chem. Solids* **37** 1135
[26] Rowe J M, Rush J J, Smith H G, Mostoller M and Flotow H E 1974 *Phys. Rev. Lett.* **33** 1297
[27] Nicol J M, Udovic T J, Rush J J and Kelly R D 1988 *Langmuir* **4** 294
[28] Jobic H, Candy J-P, Perrichon V and Renouprez A 1985 *J. Chem. Soc. Faraday Trans.* I **81** 1955
[29] Jobic H and Renouprez A 1987 *J. Less-Common Met.* **129** 311
[30] Conrad H, Kordesch M E, Scala R and Stenzel W 1986 *J. Electron. Spectrosc. Relat. Phenom.* **38** 289
[31] Conrad H, Kordesch M E, Stenzel W, Trninic-Radja B and Sunjic M 1986 *Surf. Sci.* **178** 578
[32] Ellis T H and Morin M 1989 *Surf. Sci.* **216** L351
[33] Lynch D L, Rick S W, Gomez M A, Spath B W, Doll J D and Pratt L R 1992 *J. Chem. Phys.* **97** 5177
[34] Eastman J A, Fitzsimmons M R and Thompson L J 1992 *Phil. Mag.* B **66** 667
[35] Salomons E, Griessen R, de Groot D G and Magerl A 1988 *Europhys. Lett.* **5** 449
[36] Weissmüller J 1993 *NanoStruct. Mater.* **3** 261
[37] Weissmüller J 1994 *J. Mater. Res.* **9** 4